

Spatiotemporal Variation of Water Chemistry in Meadow Run

Rachel Lombardo  
Richmond, Virginia

A Thesis presented to the Faculty of the  
University of Virginia in Fulfillment of the  
Distinguished Majors Program

Department of Environmental Sciences  
University of Virginia  
April 2024

---

Todd M. Scanlon & Ami L. Riscassi,  
Thesis Advisors

---

Robert E. Davis,  
Director of Distinguished Majors Program

**Abstract**

Meadow Run is one of the most acidified streams in Shenandoah National Park, making it a prime target for intervention to accelerate its recovery from historic acid deposition. Meadow Run has exhibited persistent acidity with low pH and acid neutralizing capacity (ANC) values as recorded by the Shenandoah Watershed Study (SWAS) from 1987 to present. To remediate this acidification, liming or the spreading of limestone sand across Meadow Run by the National Park Service (NPS) is scheduled for the winter of 2025. This study is intended to provide a thorough analysis of the stream chemistry before the liming.

In this study, the influences of the two different types of siliclastic bedrock underlying the Meadow Run watershed were assessed spatially and temporally. A spatial influence was found as areas containing a larger percentage of the Antietam Formation possessed lower ANC, pH, and base cation measurements than areas with a larger percentage of the Harpers Formation. However, with the exception of sulfate, the temporal recovery from acidification did not appear to be influenced by the bedrock geology as there were no consistent patterns for variations in ANC, pH, and base cations from 1994 to 2023. This study also investigated the spatial and temporal relationship between dissolved organic carbon (DOC) and pH as some limed watersheds have reported increases in DOC resulting from increases in pH. A statistically significant relationship was not found between pH and DOC spatially or temporally. However, this is likely due to minimal natural variation of pH and the influence of DOC by other temporal factors (e.g. hydrology) and spatial factors (e.g. soil characteristics). After the liming, this relationship will continue to be studied to determine if larger increases in pH with other factors held constant directly affect the DOC.

## Acknowledgments

I would first like to thank my research advisors, Dr. Todd Scanlon and Dr. Ami Riscassi. Undergraduate research has been my absolute favorite aspect of my education at the University of Virginia, and I feel so grateful to have worked with them over the past two years. I would like to thank Susie Maben for opening her laboratory to me and always ensuring I had everything I needed. I also want to thank her for her laboratory analysis of the bi-weekly SWAS and synoptic samplings utilized in this study. This research team has provided me with endless support and guidance. I greatly appreciate their patience and diligence, especially during the synoptic sampling where we spent a full day hiking through rapids in a snowy Meadow Run.

I want to thank my family and friends for all of their love and support throughout my undergraduate education, which kept me motivated and excited about my research. I would like to thank the University of Virginia; specifically, the Department of Environmental Sciences for establishing the Distinguished Majors Program and the Small Research and Travel Grant for their generous funding for this project. I want to thank the Undergraduate Academic Review Committee for their time, feedback, and consideration. Finally, I would also like to acknowledge the traditional custodians of the Monacan and Manahoac land in which this research was performed. I also want to recognize and honor the thousands of enslaved people who built this university where this data was analyzed.

Overall, this research experience has truly sparked my interest in water chemistry, which I plan to continue exploring in my graduate education at the University of Rochester in the Departments of Toxicology and Environmental Medicine. I am so thankful for every person's contribution and support, and I will carry the knowledge and skills from this project into my future research career.

**Table of Contents**

Abstract .....	i
Acknowledgments .....	ii
Table of Contents .....	iii
List of Figures.....	iv
1. Introduction .....	1
2. Methods .....	6
2.1 Site Description .....	6
2.2 Field and Lab Methods .....	6
2.3 Statistical Analysis.....	12
3. Results .....	13
3.1 Spatial and Temporal Influence of Bedrock Geology on Stream Chemistry.....	13
3.2 Spatial and Temporal Relationship Between pH and DOC.....	21
4. Discussion .....	25
3.1 Spatial and Temporal Influence of Bedrock Geology on Stream Chemistry.....	25
3.2 Spatial and Temporal Relationship Between pH and DOC.....	28
5. Conclusion.....	30
References .....	31
Appendix Table 1A EXO2 Sonde Calibration Parameters.....	36
Appendix Table 2A: SWAS Laboratory Procedures .....	36
Appendix Figure 1A: Silica ( $\mu\text{mol/L}$ ) from fall 1994 and fall 2023 plotted along with the difference between 2023 and 1994.....	37

## List of Figures

<b>Figure 1:</b> Meadow Run pH and ANC ( $\mu\text{eq/L}$ ) measurements from 1987-2022.....	3
<b>Figure 2:</b> Bedrock geology map of the 19 sites within the Meadow Run watershed showing the spatial distribution of the Anteitam Formation (Cca) and the Harpers Formation (Cch). An accompanying table on the right shows the %Cca area for each site.....	4
<b>Figure 3:</b> The temperature and turbidity corrected and uncorrected sonde fDOM (QSU) data plotted against the laboratory DOC values obtained from bi-weekly sampling. ....	9
<b>Figure 4:</b> Sonde vs laboratory pH measured in the field and SWAS laboratory, respectively...	10
<b>Figure 5:</b> Sonde vs laboratory specific conductivity measured in the field and SWAS laboratory respectively.....	11
<b>Figure 6:</b> Acid Neutralizing Capacity (ANC; $\mu\text{eq/L}$ ) from fall 1994 (blue) and fall 2023 (orange) plotted along with the difference between 2023 and 1994 (dark blue).....	14
<b>Figure 7:</b> pH from fall 1994 (blue) and fall 2023 (orange) plotted along with the difference between 2023 and 1994 (dark blue).....	15
<b>Figure 8:</b> Nitrate ( $\mu\text{eq/L}$ ) from fall 1994 (blue) and fall 2023 (orange) plotted along with the difference between 2023 and 1994 (dark blue).....	16
<b>Figure 9:</b> Sulfate ( $\mu\text{eq/L}$ ) from fall 1994 (blue) and fall 2023 (orange) plotted along with the difference between 2023 and 1994 (dark blue).....	17
<b>Figure 10:</b> Chloride ( $\mu\text{eq/L}$ ) from fall 1994 (blue) and fall 2023 (orange) plotted along with the difference between 2023 and 1994 (dark blue).....	18
<b>Figure 11:</b> Sum of cations ( $\mu\text{eq/L}$ ) from fall 1994 (blue) and fall 2023 (orange) plotted along with the difference between 2023 and 1994 (dark blue).....	19
<b>Figure 12:</b> Specific conductance ( $\mu\text{S/cm}$ ) from fall 1994 (blue) and fall 2023 (orange) plotted along with the difference between 2023 and 1994 (dark blue).....	20
<b>Figure 13:</b> DOC (calculated from fDOM) plotted against the pH values from the high-frequency deployment.....	21
<b>Figure 14:</b> fDOM (QSU), pH, and water level (feet) plotted against time for a storm event occurring from February 16, 2023 to February 20, 2023 (A) and April 27, 2023 to May 1, 2023 (B).....	22-23
<b>Figure 15:</b> The DOC (mg/L) plotted against the pH values from the synoptic sampling.....	24

## 1. Introduction

The emission and transport of acidifying pollutants from fossil fuel combustion known as acid deposition has resulted in the acidification of streams throughout the eastern United States (Kaufmann et al., 1991). Acid deposition results in a reduction of the stream's natural ability to buffer acidic components by depleting base cations that are derived from geological weathering (DOI, 2021). The Clean Air Act of 1970 and its amendments in 1990 were ultimately enacted to mitigate acid deposition. The Acid Rain Program (ARP) was created in 1995 to reduce nitrogen and sulfur emissions, the precursors of acid rain, from the burning of fossil fuels. A market-based cap and trade and allowance system was also created to distribute the emissions equitably based on the size of the industrial source. In 2010, a cap of 8.95 million tons was placed on sulfur dioxide emissions, which was a reduction of 10 million tons compared to 1980 (EPA 2010, Harmon et al., 2021). Although this legislation placed restrictions on the emissions of these pollutants, model projections reflect that even with the most stringent regulations, the chemistry and wildlife in these streams will not recover from historic acidification until beyond the year 2200 (Shao et al., 2020).

Since reductions in emissions can only prevent the worsening of already acidified streams, methods of remediating previous acidification are necessary to explore. One method known as liming was initially utilized as a means of preventing further acidification with continued unregulated fossil fuel emissions but is now being explored for its potential to decrease the acidity of streams (Lawrence et al., 2016). Liming is the spreading of limestone sand or pellets across a soil or stream to raise the pH. After the establishment of the Clean Air Act, liming as a preventive measure was no longer necessary since the surface water chemistry and soil chemistry of many streams began to naturally recover. However, some streams lagged in

their recovery due to underlying bedrock geology, which contributes to the natural buffering capacity of a watershed's soils. Thus, liming was explored as a means of accelerating this recovery in many locations throughout Europe and in some locations throughout North America (Lawrence et al., 2016; Millard et al., 2018). Although lime applications have the general desired effect of increasing the pH of the stream of study, increases in pH are often accompanied by a variety of other changes including increases in DOC, total mercury, and methylmercury (Millard et al., 2018). Previous studies have indicated that the natural acidity of a stream is related to the quantity and character of DOC, with more acidic watersheds exhibiting lower concentrations and less aromatic DOC. The character of DOC is significant as greater aromaticity is correlated to increased mobilization of mercury (Riscassi and Scanlon, 2011).

Meadow Run in Shenandoah National Park is particularly sensitive to acid deposition as it is underlain by siliciclastic bedrock that naturally has fewer base cations than other types of bedrock (DOI, 2021). The pH and ANC values of under 6.0 and 50  $\mu\text{eq/L}$ , respectively, of Meadow Run indicate that it has remained persistently acidic since the late 1980s, placing Meadow Run on the impaired waters list under Section 303d of the Clean Water Act (CWA) (Riscassi et al., 2020; VADEQ 2020) (Figure 1).

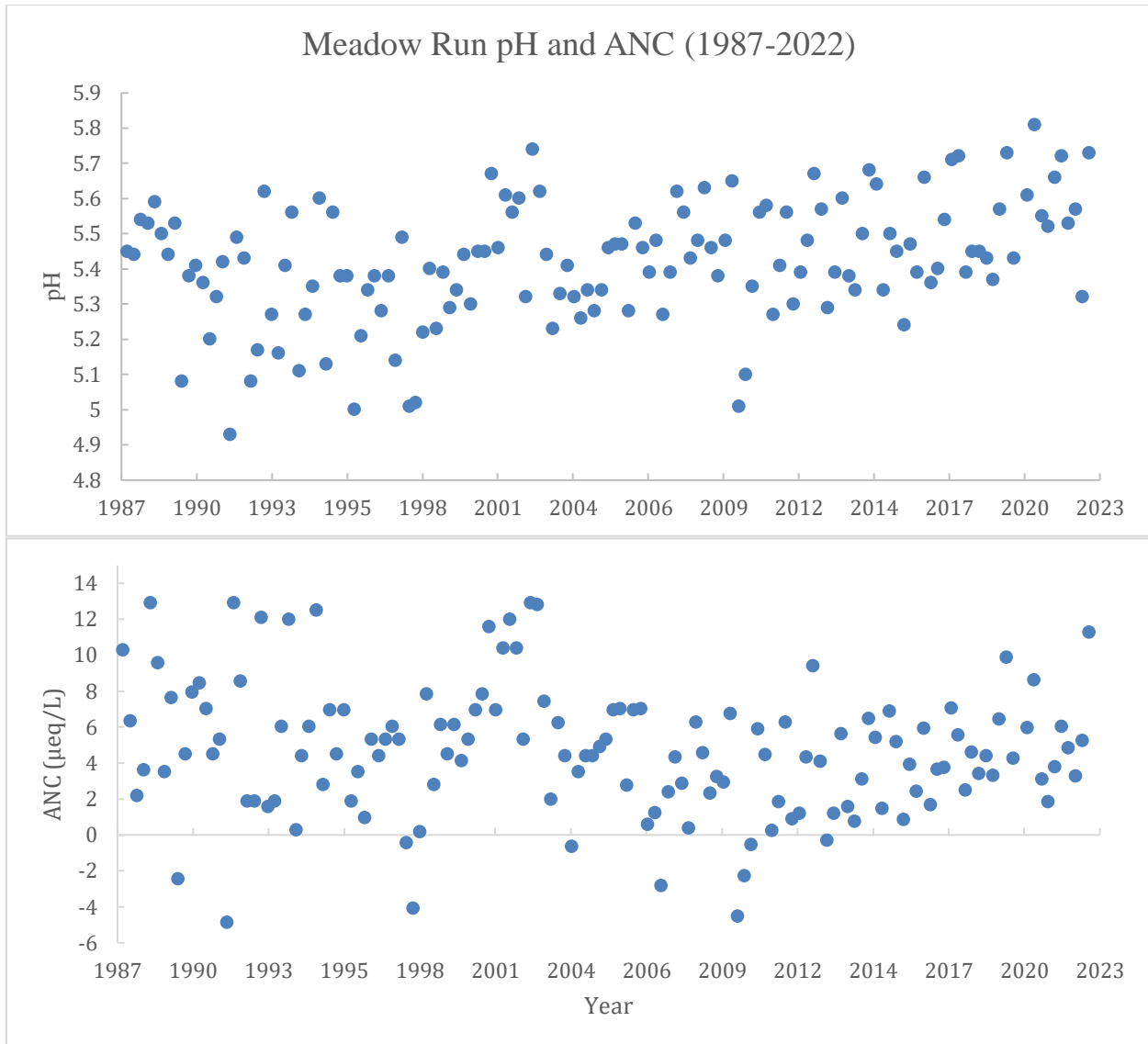


**Figure 1:** Meadow Run pH and ANC ( $\mu\text{eq/L}$ ), measured at site VT36, from 1987-2022

Meadow Run is underlain by two types of bedrock, the Antietam Formation, which composes the western portion of the watershed, and the Harpers Formation, which composes the eastern portion (Sharpe and Cummings, 2019; DOI, 2021) (Figure 2). The Antietam Formation has been found to release fewer base cations, giving it a lower overall ANC. Thus, the western region of the watershed is expected to be more acidic. The lack of ability to neutralize acidic components has diminished the survival of many species of fish, other aquatic organisms,

insects, birds, and numerous plants that cannot withstand such acidity (Graveland, 1998; Bulger et al., 1999; Burns et al., 2011; Jastram, 2013).

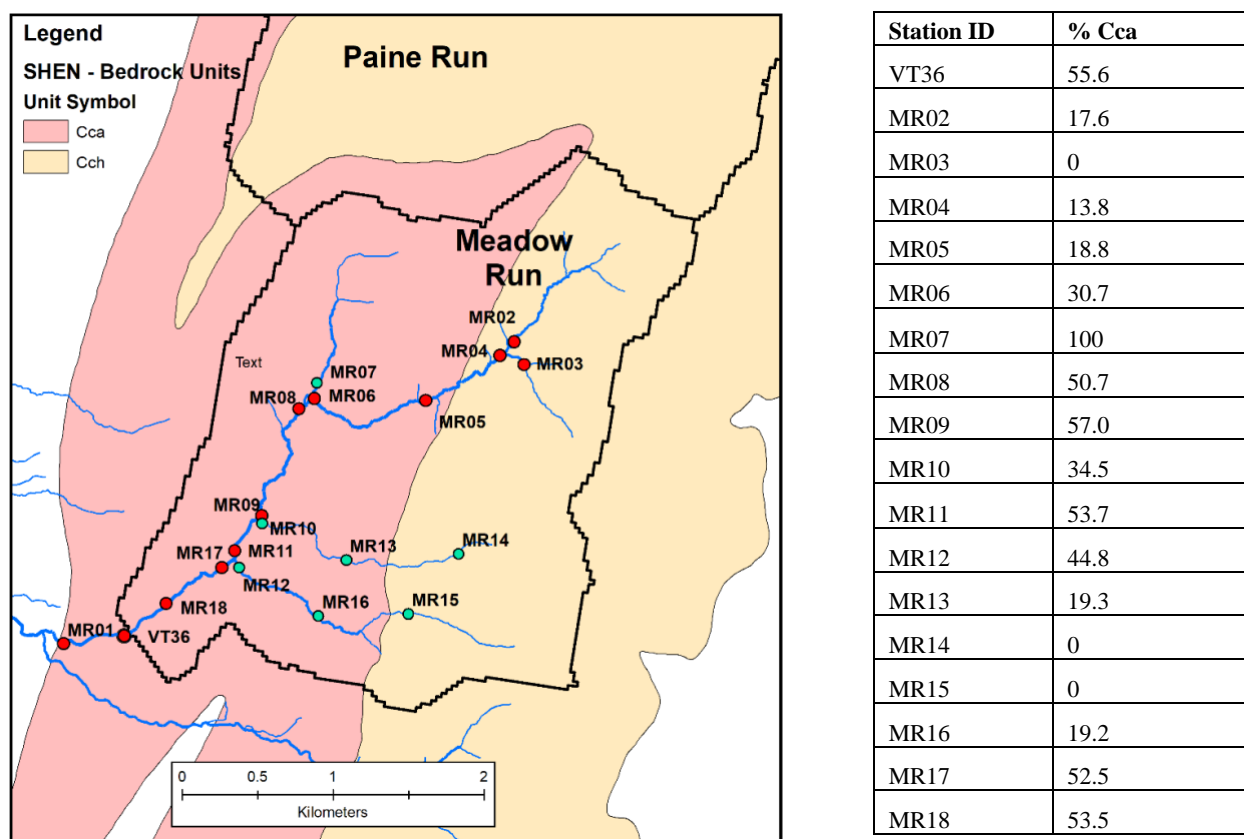


**Figure 2:** Bedrock geology map of the 19 sites within the Meadow Run watershed showing the spatial distribution of the Antietam Formation (Cca) and the Harpers Formation (Cch). An accompanying table on the right shows the %Cca area for each site. The Sites MR01 and MR05 were excluded from comparison as these were only sampled in the fall of 2023. Sampling sites are located on the main channel (red circles) and tributaries (green circles).

Due to the persistent acidity of Meadow Run, the National Park Service (NPS) has scheduled a liming application for the early winter of 2025. This liming will include the spreading of limestone sand by helicopter with either an even distribution across the watershed or tailored distributions based on the more and less acidic regions (DOI, 2021). Meadow Run has been monitored quarterly (1987-present) at the outlet (VT36) and sampled spatially with several synoptic samplings in the mid-1990s. To gain a better understanding of the pre-liming chemistry, stream sampling by the SWAS laboratory was increased to weekly in 2022 and high-frequency

data collection with the use of an in-situ water-quality measurement device was established in the spring of 2023. For this project, high-frequency datasets were collected from spring 2023 to winter 2024, and synoptic data was obtained in fall 2023.

The purpose of this project is to document the stream chemistry of Meadow Run before the liming, which will aid in determining the impacts of the liming. I aim to answer two main research questions. 1) How have differences in bedrock geology influenced temporal changes in stream chemistry within the Meadow Run watershed? I hypothesized that the western region underlain with the Antietam Formation would experience greater acidity as denoted by lower pH, lower ANC, and lower base cation content than the eastern region underlain with the Harpers Formation and that over time, the eastern region would exhibit a greater recovery. 2) Do the spatial patterns of the relationship between pH and DOC conform with the temporal relationships observed at the watershed outlet? I predicted that naturally more acidic regions would have lower concentrations of DOC than naturally less acidic regions and that this relationship would also be reflected in variations of acidity measured by continuous sampling at one location. Although the intended consequence of liming is increasing the pH of the stream, it may also result in the unintended consequence of increasing the DOC content, which has implications for mercury mobilization. Thus, evaluating the influence of the underlying bedrock geology and the relationship between pH and DOC before the liming lends to a better understanding of the potential effects of the liming on the stream chemistry and ultimately provides insights into the ecosystem health of Meadow Run.

## 2. Methods

### 2.1 Site Description

Meadow Run is a tributary of the South River that travels into the South Fork of the Shenandoah River. Its headwaters are in the south district of Shenandoah National Park (SHEN). Within SHEN, the Meadow Run watershed has an area of 8.7 km<sup>2</sup> and ranges in elevation from 467 m at the base to a maximum of 925 m along the ridge. The entire area of Meadow Run to be limed is forested with the dominant and codominant plant species compositions of 55% chestnut oak (*Quercus prinus*) and red oak (*Quercus rubra*), 21% sweet birch (*Betula lenta*) and chestnut oak, 17% table mountain pine (*Pinus pungens*), pitch pine (*Pinus rigida*), and chestnut oak, 3% mixed hardwoods including yellow birch (*Betula alleghaniensis*), sugar maple (*Acer saccharum*), hemlock (*Tsuga canadensis*), and 4% catastrophically disturbed forest with greater than 75% canopy mortality from the spongy moth, fires, and hemlock wooly adelgid (DOI 2021). This watershed is of particular interest as it is underlain with two types of siliciclastic bedrock: the Harpers Formation (Cch) and the Antietam Formation (Cca) (Figure 2). There are four main tributaries feeding into the main stem of the stream. One of these tributaries is composed entirely of Cca while the other three are composed largely of Cch. Of the two types of bedrock, Cca has the lowest acid neutralizing capacity (Riscassi et al, 2020; DOI, 2021).

### 2.2 Laboratory and Field Methods

Two methods of stream water data collection were employed: high-frequency in-situ measurements at a single location every 15 minutes using a multivariable water quality sonde (YSI EXO2, Yellow Springs, Ohio), and synoptic sampling where grab samples were obtained from 19 different sites throughout the watershed and analyzed in the SWAS laboratory. For the high-frequency sampling, the sonde was deployed with five different sensors attached. These

sensors measured optical dissolved oxygen (ODO) in percent saturation, temperature in degrees Celsius ( $^{\circ}\text{C}$ ), specific conductivity in microsiemens per cm ( $\mu\text{S}/\text{cm}$ ), turbidity in Formazin Nephelometric Units (FNU), pH, and fluorescent dissolved organic matter (fDOM) in Quinine Sulfate Units (QSU). The sensors were calibrated with known standards according to manufacturer instructions (YSI, 2020). The specific calibration points for each sensor are outlined in Table 1A. The high-frequency deployment involved submerging the sonde from February 6, 2023 to January 22, 2024 with removals every 2-3 months for battery replacement, sensor reading accuracy checks, and recalibration.

To determine the reliability of the high-frequency sonde data, stream samples that were collected every two weeks and analyzed in the SWAS laboratory for DOC, specific conductivity, and pH were compared to concurrent in-situ measurements. Although fDOM has been cited as an accurate proxy for DOC, it can vary depending on the temperature and turbidity conditions of the environment in which the sensor is deployed. Temperature and fDOM have an inverse relationship. At higher temperatures, it is more likely for a particle to return to its ground state from an excited state by radiationless decay, which decreases the intensity of the fluorescence and thus the fDOM measurement. To account for this effect, a correction known as the temperature-specific fluorescence coefficient can be applied which normalizes the temperature to standard conditions ( $25\text{ }^{\circ}\text{C}$ ). This correction was implemented by a published equation that also accounts for turbidity (Watras et al., 2011; Downing et al., 2012)

$$[1] \text{fDOM}_{\text{corrected}} = \text{fDOM}_{\text{measured}} + [\rho \cdot (T_{\text{measured}} - T_{25})] / [r_p \cdot (\text{FNU})]$$

Where  $\text{fDOM}_{\text{measured}}$  is the raw fDOM value obtained from the sonde (QSU),  $\rho$  is the temperature-specific coefficient of fluorescence ( $-0.012\text{ }^{\circ}\text{C}^{-1}$ ),  $T_{\text{measured}}$  is the raw temperature value obtained from the sonde ( $^{\circ}\text{C}$ ),  $r_p$  is the instrument-specific correction constant for dissolved

and suspended particles (0.15), and FNU is the raw turbidity value measured by the sonde. The values of  $\rho$  and  $r_p$  were obtained from a published study in which a river was monitored with the use of a YSI EXO fDOM sensor. This study found an average  $r_p$  value of 0.15 by comparing the fDOM readings of unfiltered samples to filtered samples. Since the environment was similar to the Meadow Run catchment and the same instrument was used for measurements, the temperature and turbidity correction constants were applied to the fDOM data in this study. This publication applied the turbidity correction to the range of 22 to 46 FNU, citing that at lower turbidity concentrations, the interference with fDOM measurement is negligible (Hoffmeister et al., 2020). Following these guidelines, the range of temperature and turbidity conditions over which these corrections were applied included 1.805 to 20.382 °C for temperature and 25.68 to 27.96 FNU for turbidity.

When comparing the field fDOM values to the laboratory DOC concentrations, a strong linear relationship was found for both the corrected and uncorrected fDOM values (corrected: slope = 11.588 QSU/mg/L,  $R^2 = 0.9448$ ; uncorrected: slope = 11.524 QSU/mg/L,  $R^2 = 0.9432$ ) (Figure 3). The equation for this relationship was applied to the remaining fDOM data to estimate DOC concentrations on a continuous basis.

$$[2] \text{DOC}_{\text{fDOM}} = (\text{fDOM}_{\text{measured}} + 3.0643) / 11.588$$

Where  $\text{DOC}_{\text{fDOM}}$  is the DOC values obtained from the fDOM values measured by the sonde ( $\text{fDOM}_{\text{measured}}$ ).

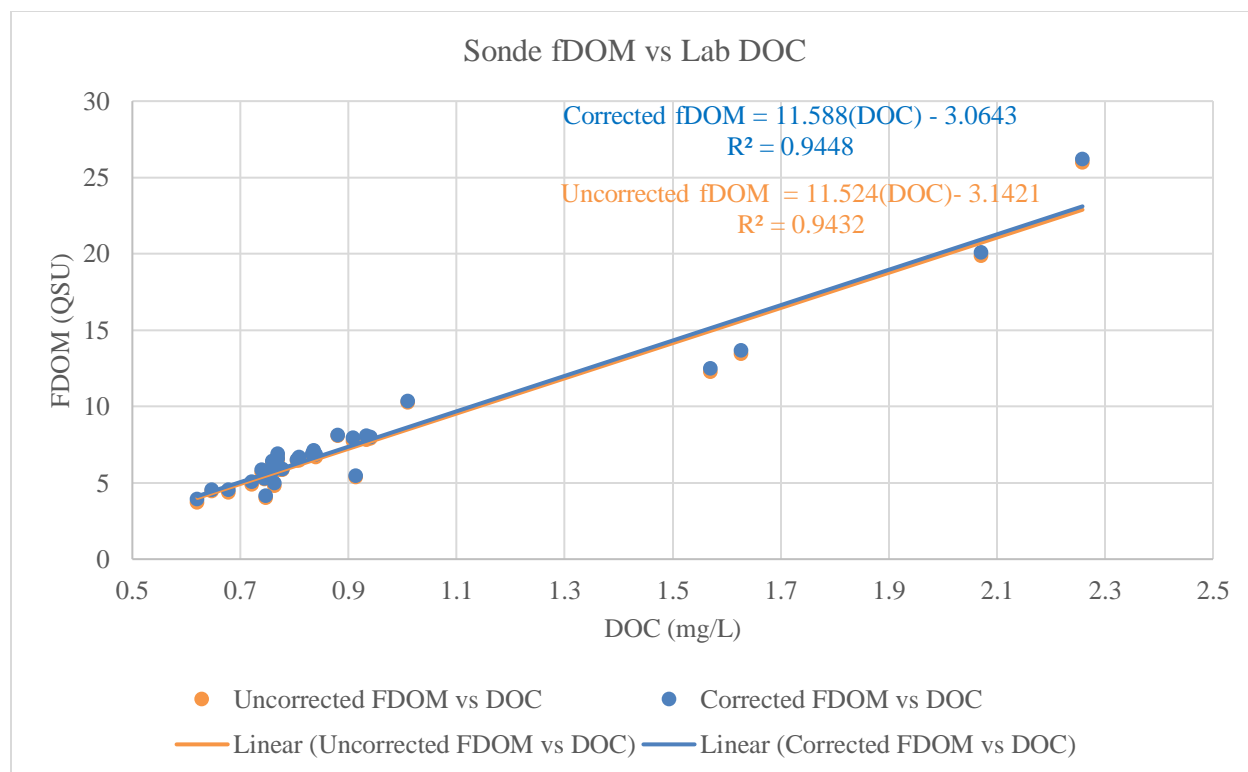


**Figure 3:** The temperature and turbidity corrected and uncorrected sonde fDOM (QSU) data plotted against the laboratory DOC values obtained from bi-weekly sampling. The R<sup>2</sup> value for the uncorrected fDOM was 0.9432 while the corrected had a value of 0.9448.

For the field and laboratory pH measurements, there was a weak linear relationship and a matched pairs T test reflected that the difference was statistically significant (slope=0.0208, R<sup>2</sup>=0.0012, p=0.017) (Figure 4). However, the acceptable error range for sonde measurements is pH  $\pm$ 0.3 while that of the laboratory probe is 0.075 (pH $\leq$ 5.75) or 0.15 (pH $>$ 5.75). The most significant difference between field and lab pH measurements was 0.38 (5.22, 5.60), which is close to the acceptable error range. Additionally, published guidelines have noted that pH samples from the field must be analyzed within 2 hours of collection (APHA, 1992). Otherwise, these samples are more susceptible to CO<sub>2</sub> degassing, which effectively lowers the pH. It was found that the laboratory measurements typically fell below the field measurements. In the SWAS laboratory, the samples are preserved within a few hours and analyzed within 2-3 days.

Over this period, it is possible for CO<sub>2</sub> degassing to occur, contributing to the observed discrepancies.

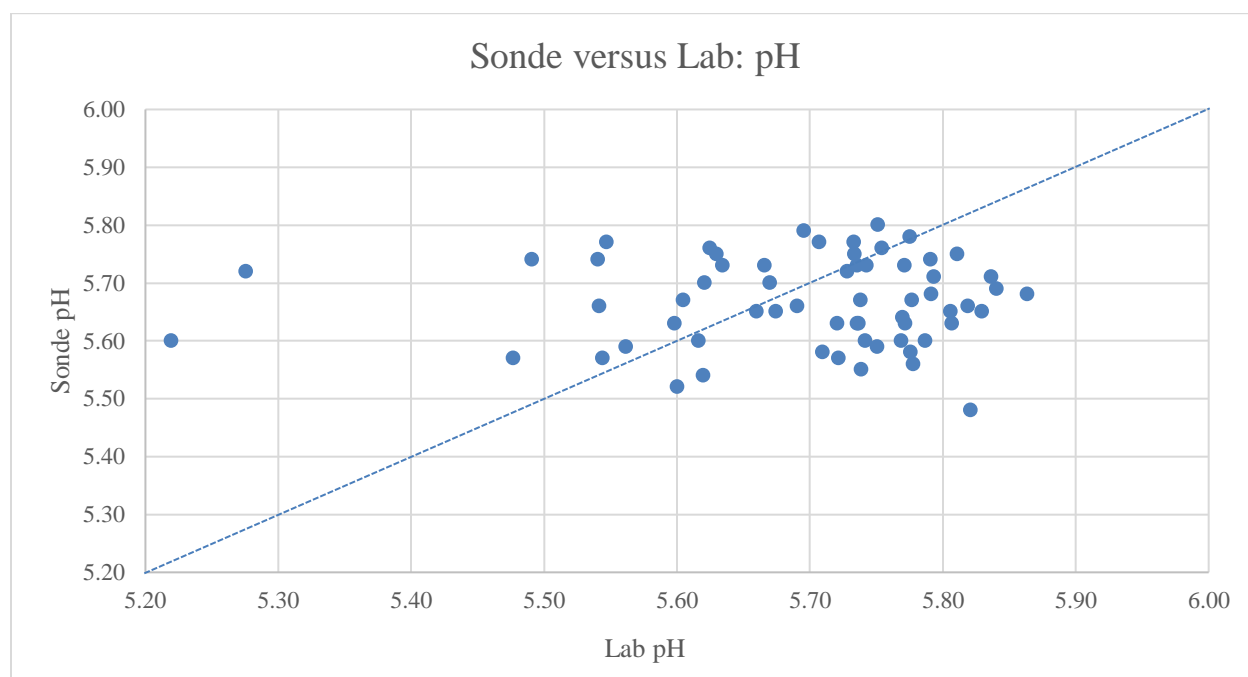


**Figure 4:** Sonde vs laboratory pH measured in the field and SWAS laboratory, respectively. The acceptable error range for the sonde pH is  $\pm 0.3$ , and the error for the laboratory probe is  $\pm 0.075$  for measurements below or equal to 5.75 and  $\pm 0.15$  for measurements above 5.75 (Wagner et al, 2006; Paulsen, 1997).

For the field and laboratory specific conductivity measurements, there was a moderate linear trend and the matched T test demonstrated that there was not a significant difference (slope=0.8891,  $R^2=0.5464$ ,  $p=0.749$ ) (Figure 5). The measurement uncertainties for these data were  $\pm 0.5$  or 3% of the measurements for the sonde and  $\pm 0.10$  for the laboratory probe. Most measurements fell within the acceptable error range for specific conductivity.

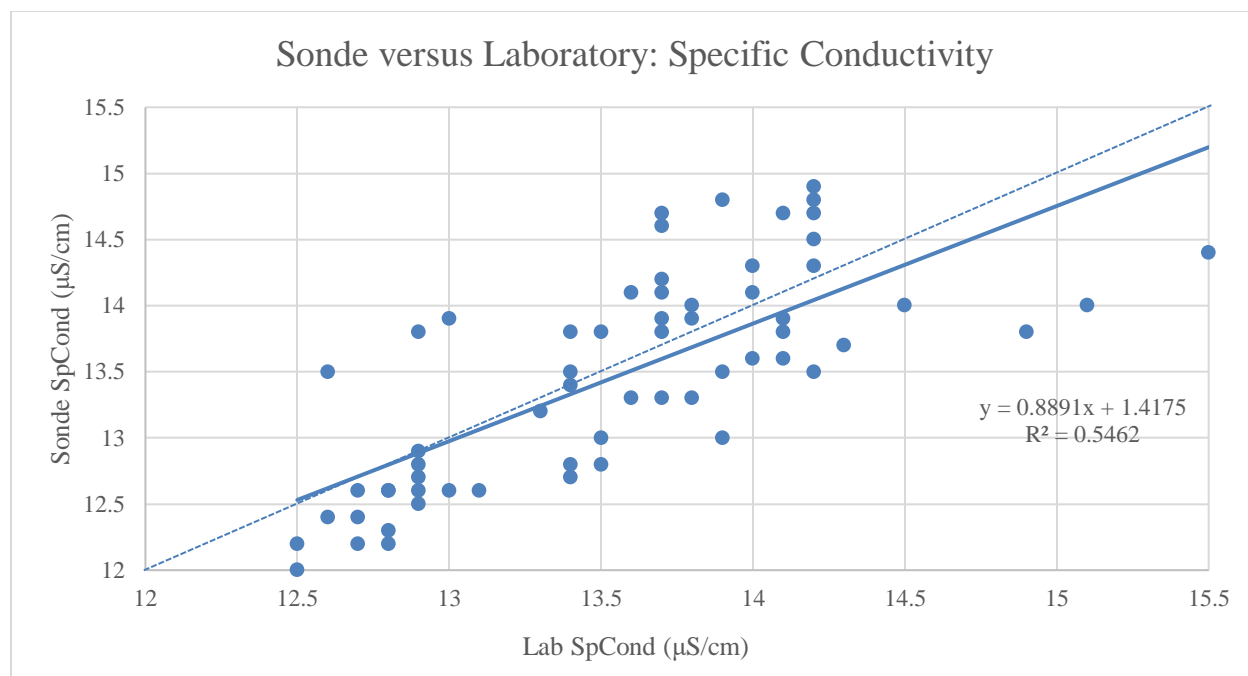


**Figure 5:** Sonde vs laboratory specific conductivity measured in the field and SWAS laboratory, respectively. The acceptable error range for the sonde specific conductivity is  $\pm 0.5$   $\mu\text{S}/\text{cm}$  or 3% of the measurement, and the error for the laboratory probe is  $\pm 0.10$   $\mu\text{S}/\text{cm}$  for measurements below 50  $\mu\text{S}/\text{cm}$  (Wagner et al, 2006; Paulsen, 1997).

For the synoptic sampling, grab samples were collected from 19 stream sites throughout the watershed (Figure 2). The synoptic grab samples were analyzed for ANC ( $\mu\text{eq}/\text{L}$ ), pH, base cations ( $\mu\text{eq}/\text{L}$ ), acid anions ( $\mu\text{eq}/\text{L}$ ), silica ( $\mu\text{mol}/\text{L}$ ), and DOC ( $\text{mg}/\text{L}$ ; 2023 only) by the methods outlined in Table 2A. A dataset for the fall of 1994 (November 1, 1994) was previously collected by SWAS and a recent synoptic sampling was performed in the fall of 2023 (December 14, 2023). In total, 17 identical sites were analyzed in the fall of 1994 and 2023. To obtain the percentage of bedrock formation contained by each sub-watershed, Meadow Run was delineated using ArcGIS Pro. The coordinates for each site were imported and each sub-watershed was generated from a pour point snapped from the flow accumulation map. The sub-watersheds were then converted to polygons, and the bedrock geology map, obtained from the U.S. Geological Survey, was clipped to each polygon. The areas for the Harpers and Antietam formations were then obtained from the attribute table for each geology clip to determine the percentage of each in the sub-watersheds (Figure 2).

### ***2.3 Statistical Analysis***

For each analyte from the synoptic samplings, graphs were generated in Excel with the data plotted for both 1994 and 2023 against the percentage of Cca. An additional plot was also generated with the difference in values between 1994 and 2023 against the percentage of Cca. For each plot, the site, VT36, is labeled as a triangle instead of a circle to mark the location of the sonde deployment for high-frequency data collection. The error bars representing analytical uncertainty were added based on the average uncertainty associated with each analyte measured by SWAS in 2022. Differences were not considered significant if the analytical uncertainty overlapped with zero. The DOC calculated from the fDOM data was plotted against the pH from the high-frequency dataset and the DOC was plotted against the pH from the fall of 2023 synoptic dataset in Excel. For the synoptic data set, simple linear regression analysis was performed in Excel to determine the  $R^2$ , slope, and p-values associated with the linear correlation. The ranges of those regressions and the outliers calculated from the interquartile method of outlier detection were determined in RStudio. Relationships were considered significant if  $p < 0.05$ . To avoid autocorrelation and meet the assumptions of linear regression in the high-frequency dataset, 19 random data points were selected repeatedly and slopes of the linear regressions for each set of values were determined in Excel. A T-test on the population of slopes was performed to determine if the mean was different than zero, indicating a significant relationship.

### 3. Results

#### *3.1 Spatial and Temporal Influence of Bedrock Geology on Stream Chemistry*

To address the first research question regarding the influence of the bedrock geology on stream chemistry and recovery from acid deposition within the Meadow Run watershed, the percentage of the Antietam Formation (Cca) for each of the 17 sub-watersheds was plotted against the analyte concentrations obtained from November 1, 1994 (fall 1994) and December 14, 2023 (fall 2023) along with the differences in concentrations between the two time periods (fall 2023 minus fall 1994). The range of Cca bedrock was from 0% for the sites MR03, MR14, and MR15 to 100% for MR07, which are all located in tributaries branching from the main stem (Figure 2).

The difference in ANC values from 1994 to 2023 did not appear to follow a consistent trend with the bedrock geology as most sites from 20-100% Cca demonstrated a similar magnitude of increase. The overall range of ANC values was from -3.17 to 24.61  $\mu\text{eq/L}$  for 1994 and -1.59 to 24.61  $\mu\text{eq/L}$  for 2023. In both years, the minimum ANC was observed at the site containing 100% Cca and the maximum at a site containing 20% Cca (Figure 6). ANC differences ranged from a decrease of 12.19  $\mu\text{eq/L}$  at a site containing 0% Cca to an increase of 1.97  $\mu\text{eq/L}$  at a site containing 31% Cca. Most sites under 20% Cca showed an increase while the others demonstrated a decrease and two sites with approximately 55% Cca showed no significant change.

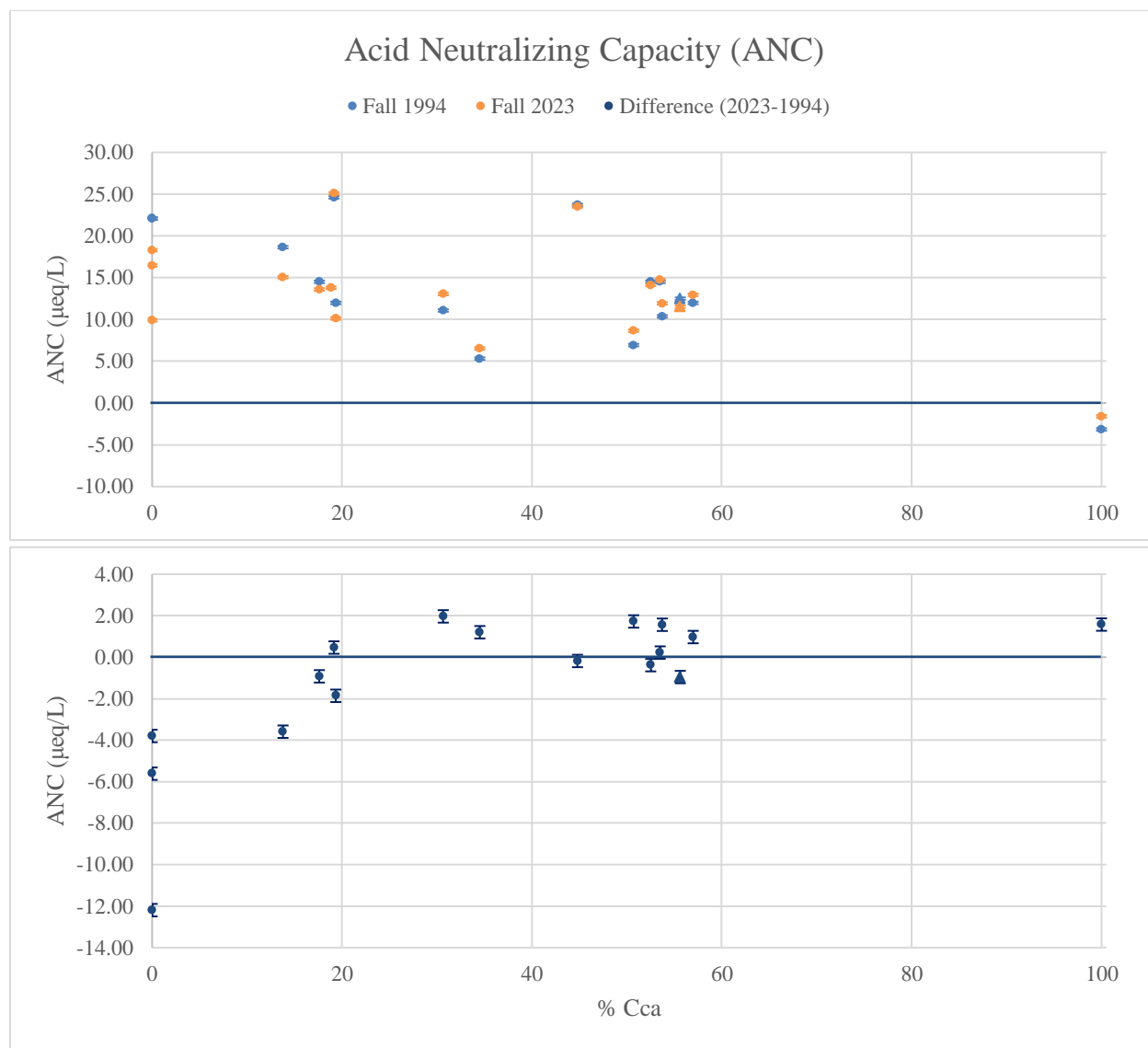


**Figure 6:** Acid neutralizing capacity (ANC;  $\mu\text{eq/L}$ ) from fall 1994 (blue) and fall 2023 (orange) plotted along with the difference between 2023 and 1994 (dark blue) against the percentage of Cca. The error bars of  $\pm 0.15 \mu\text{eq/L}$  for fall 1994 and 2023 were obtained from the average values for 2022. The error bars for the difference were the sum of the fall 1994 and 2023 error values. The triangles represent site VT36 where the high-frequency data has been collected.

There was an increase in pH from 1994 to 2023 at all sites (Figure 7). The range of pH values observed was from 4.94 to 5.80 in 1994 and 5.12 to 6.07 in 2023 with all sites demonstrating a significant increase from 1994 to 2023. The maximum pH was a site containing 19% Cca for 1994 and 45% for 2023. The minimum pH was reported at the site containing 100% Cca for both years. For two of the sites containing 0% Cca, there was a relatively large increase



nitrate concentrations were observed at the sites containing 20% Cca for 1994 and 0% for 2023. Within the 20-100% Cca range, many sites possessed values close to 0  $\mu\text{eq/L}$ . The largest increase of 25.33  $\mu\text{eq/L}$  was observed at a site containing 0% Cca while the largest decrease of -5.09  $\mu\text{eq/L}$  was observed at a site containing 18% Cca.

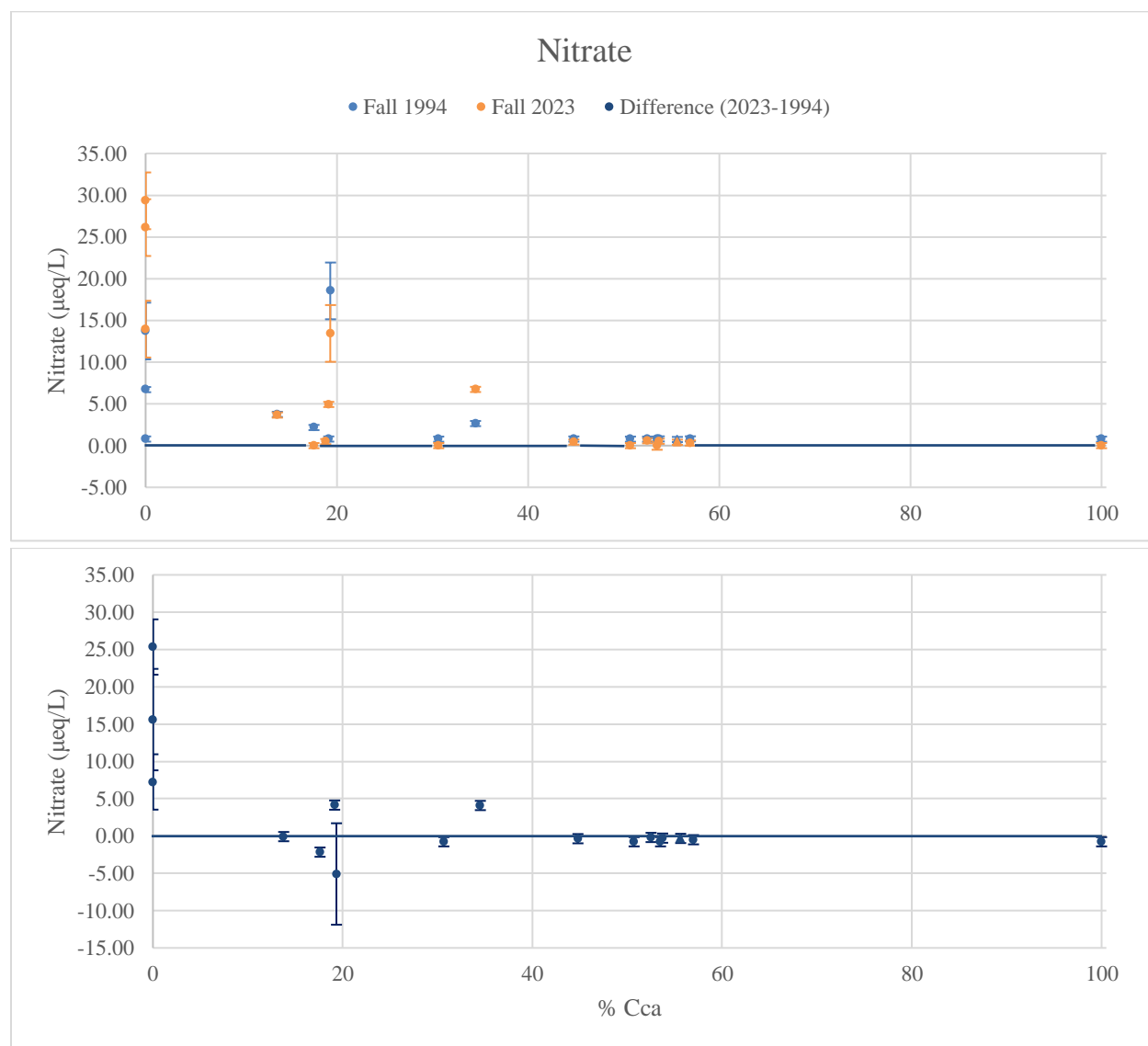


**Figure 8:** Nitrate ( $\mu\text{eq/L}$ ) from fall 1994 (blue) and fall 2023 (orange) plotted along with the difference between 2023 and 1994 (dark blue) against the percentage of Cca. The error bars of  $\pm 0.31$   $\mu\text{eq/L}$  ( $\leq 10$   $\mu\text{eq/L}$ ) and  $\pm 3.40$  ( $> 10$   $\mu\text{eq/L}$ ) for fall 1994 and 2023 were obtained from the average values for 2022. The error bars for the difference were the sum of the fall 1994 and 2023 error values. The triangles represent site VT36 where the high-frequency data has been collected.

Sulfate concentrations decreased among most of the sites except those containing 0% Cca, which experienced increases (Figure 9). The range of sulfate concentrations was 56.89 to

93.67  $\mu\text{eq/L}$  observed in 1994 and 48.09 to 97.80  $\mu\text{eq/L}$  in 2023. The site with the maximum sulfate concentration for both years contained 0% Cca while the sites with the minimum sulfate concentrations contained 18% Cca for 1994 and 100% Cca for 2023. The site that demonstrated the greatest decrease of 19.59  $\mu\text{eq/L}$  contained 100% Cca while the site that possessed the greatest increase of 4.13  $\mu\text{eq/L}$  contained 0% Cca.

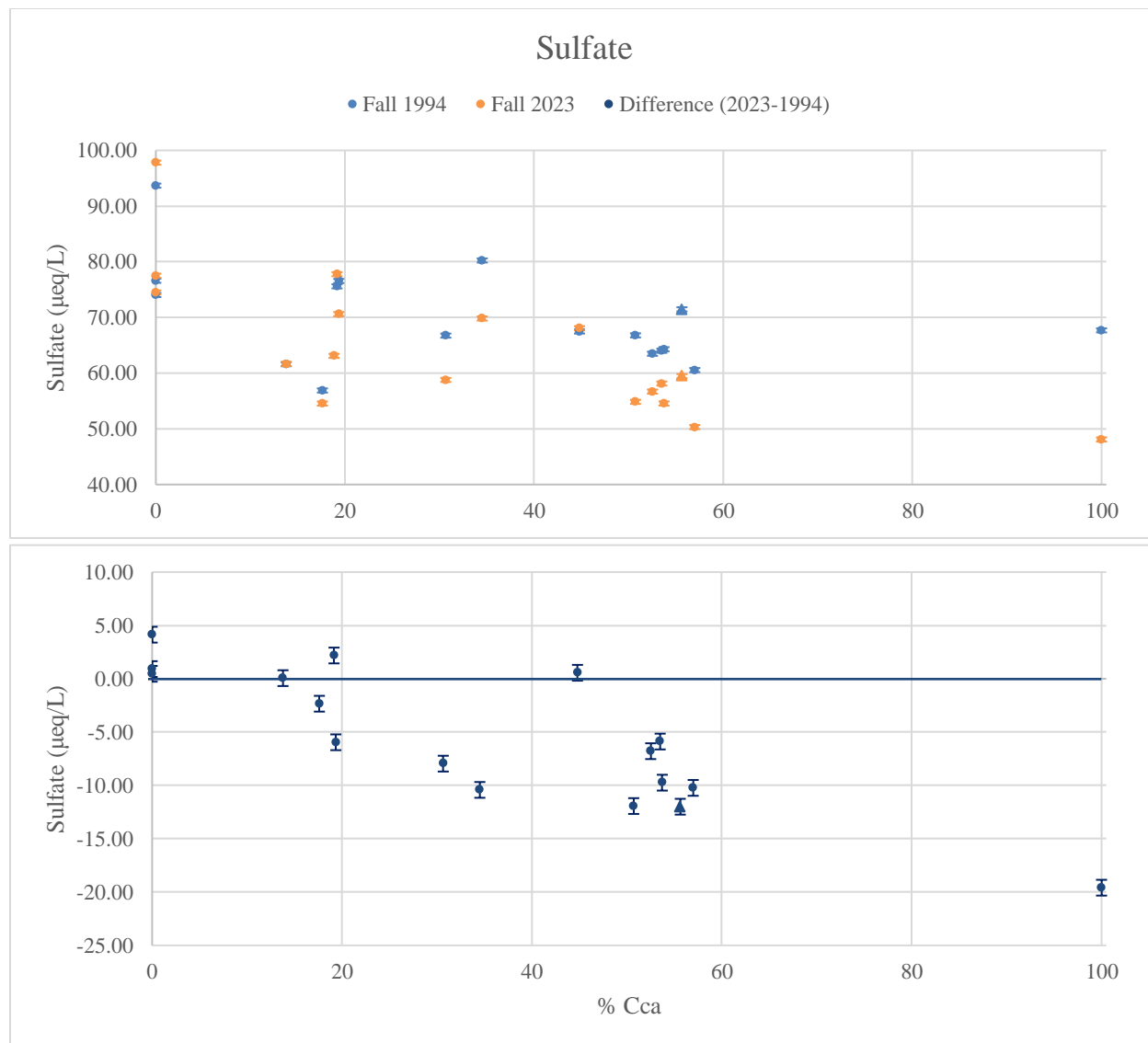


**Figure 9:** Sulfate ( $\mu\text{eq/L}$ ) from fall 1994 (blue) and fall 2023 (orange) plotted along with the difference between 2023 and 1994 (dark blue) against the percentage of Cca. The error bars of  $\pm 0.08$   $\mu\text{eq/L}$  ( $\leq 20$   $\mu\text{eq/L}$ ) and  $\pm 0.37$  ( $> 20$   $\mu\text{eq/L}$ ) for fall 1994 and 2023 were obtained from the average values for 2022. The error bars for the difference were the sum of the fall 1994 and 2023 error values. The triangles represent site VT36 where the high-frequency data has been collected.

All sites showed a statistically significant decrease in chloride concentration from 1994 to 2023 with the range of 23.78 to 31.03  $\mu\text{eq/L}$  in 1994 changing to 20.22 to 23.48  $\mu\text{eq/L}$  by 2023 (Figure 10). The sites with the maximum chloride concentrations were those containing 0% for 1994 and 51% for 2023, while the minimum chloride concentrations were those containing 56% for 1994 and 100% for 2023. A site containing 0% Cca showed the largest decrease of 10.26  $\mu\text{eq/L}$  while a site containing 51% Cca showed the smallest decrease close to 2.37  $\mu\text{eq/L}$ .

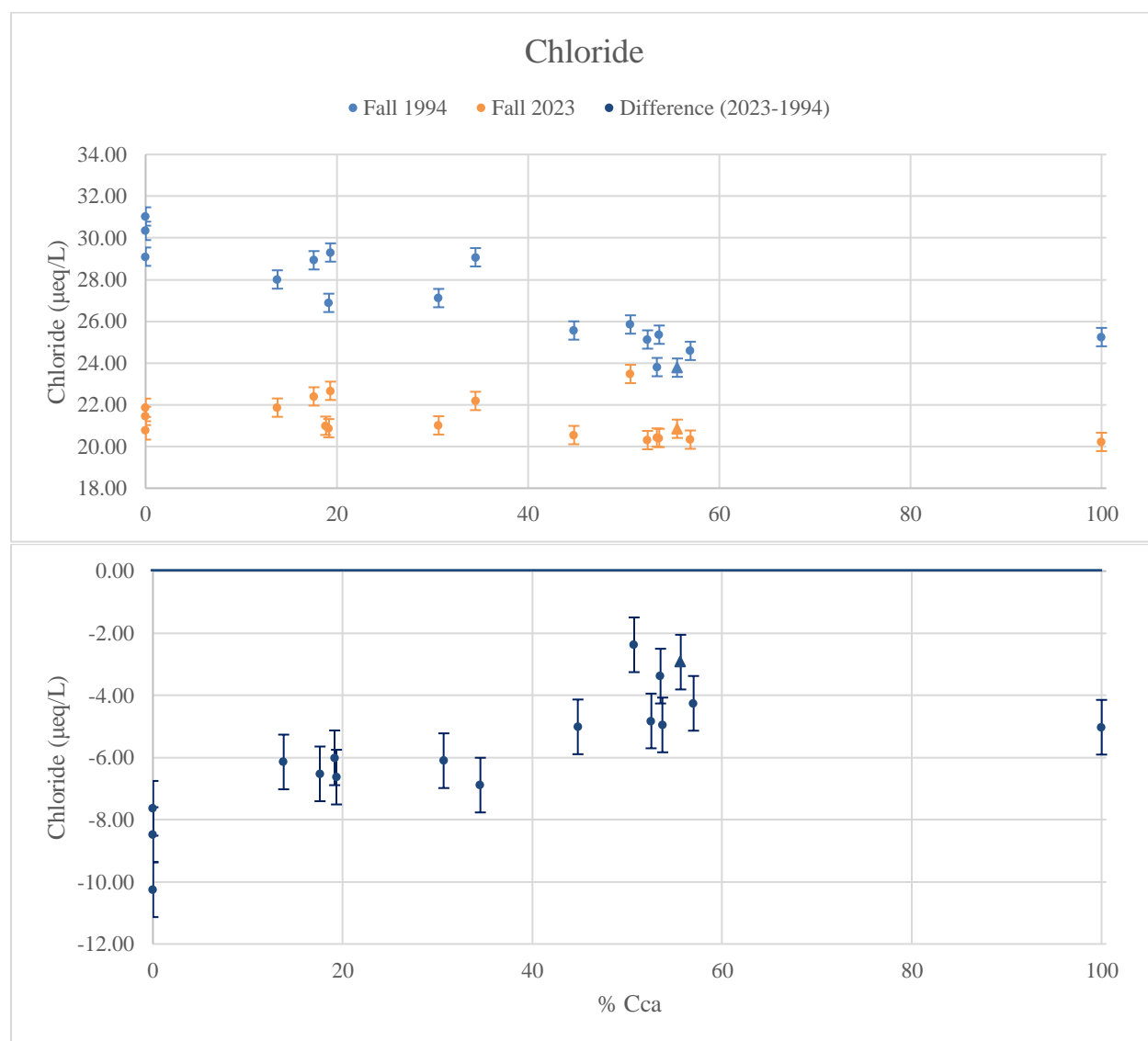


**Figure 10:** Chloride ( $\mu\text{eq/L}$ ) from fall 1994 (blue) and fall 2023 (orange) plotted along with the difference between 2023 and 1994 (dark blue) against the percentage of Cca. The error bars of  $\pm 0.06$   $\mu\text{eq/L}$  ( $\leq 20$   $\mu\text{eq/L}$ ) and  $\pm 0.44$  ( $> 20$   $\mu\text{eq/L}$ ) for fall 1994 and 2023 were obtained from the average values for 2022. The error bars for the difference were the sum of the fall 1994 and 2023 error values. The triangles represent site VT36 where the high-frequency data has been collected.

The sum of base cations generally demonstrated a significant change from 1994 to 2023. Most sites decreased with an exception at 0% Cca which increased by 14.54  $\mu\text{eq/L}$  (Figure 11). The range of concentrations was 81.83 to 157.97  $\mu\text{eq/L}$  in 1994 and 61.62 to 174.26  $\mu\text{eq/L}$  in 2023. The site with the maximum concentration was 0% Cca for both 1994 and 2023 and the site with the minimum concentration was 100% Cca for both 1994 and 2023. Although the decreases were similar in magnitude, the site with 100% Cca had the greatest decrease of 20.21  $\mu\text{eq/L}$ .

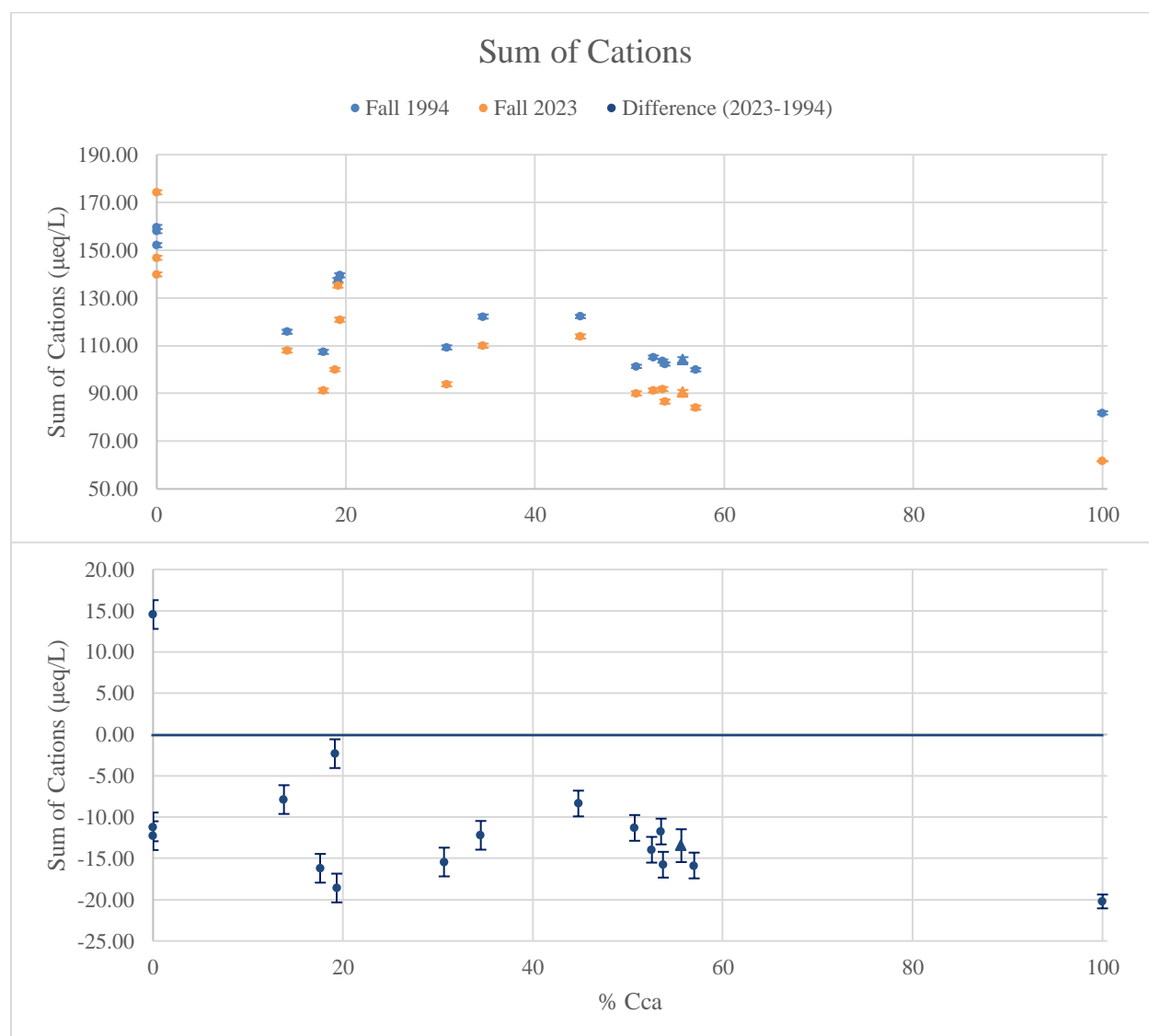


**Figure 11:** Sum of cations ( $\mu\text{eq/L}$ ) from fall 1994 (blue) and fall 2023 (orange) plotted along with the difference between 2023 and 1994 (dark blue) against the percentage of Cca. The error bars for fall 1994 and 2023 were obtained from the sum of average values for 2022 for each of the base cations including calcium, potassium, sodium, and magnesium. The error bars for the difference were the sum of the fall 1994 and 2023 error values. The triangles represent site VT36 where the high-frequency data has been collected.

The specific conductance for all sites generally decreased from 1994 to 2023 except for two sites containing below 20% Cca (Figure 12). The range of values was from 13.71 to 20.78  $\mu\text{S}/\text{cm}$  in 1994 and 11.60 to 23.00  $\mu\text{S}/\text{cm}$  in 2023. The site with the maximum specific conductance contained 0% Cca for both years while the site with the minimum specific conductance contained 57% Cca for both years. The largest decrease of 3.79  $\mu\text{S}/\text{cm}$  was the site containing 100% Cca and the largest increase of 1.74  $\mu\text{S}/\text{cm}$  was the site containing 0% Cca.

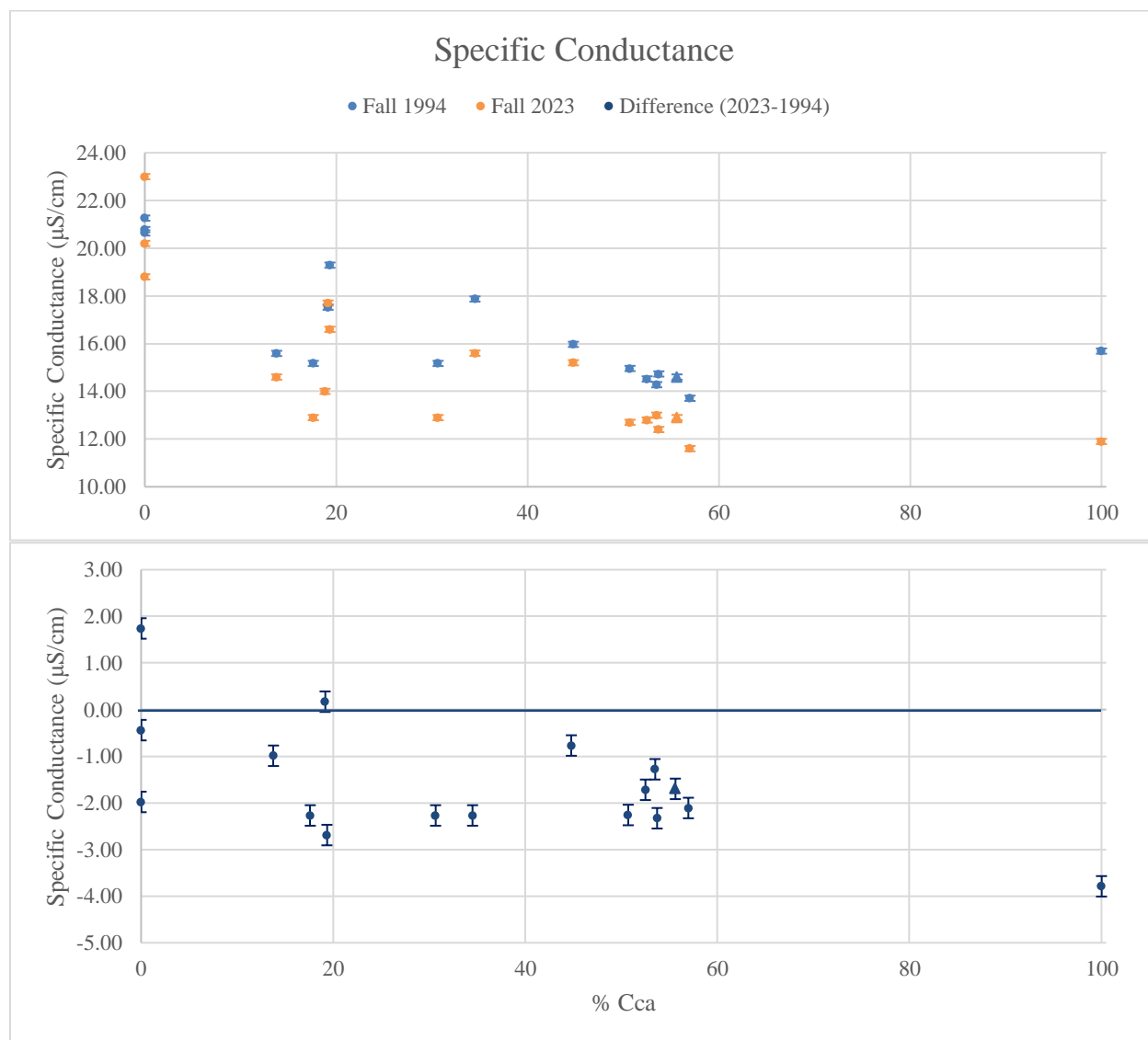


**Figure 12:** Specific conductance ( $\mu\text{S}/\text{cm}$ ) from fall 1994 (blue) and fall 2023 (orange) plotted along with the difference between 2023 and 1994 (dark blue) against the percentage of Cca. The error bars of  $\pm 0.11 \mu\text{eq}/\text{L}$  ( $\leq 50 \mu\text{eq}/\text{L}$ ) for fall 1994 and 2023 were obtained from the average values for 2022. The error bars for the difference were the sum of the fall 1994 and 2023 error values. The triangles represent site VT36 where the high-frequency data has been collected.

The chemical parameter silica was also measured, which is indicative of the amount of weathering experienced by the watershed. Silica did not appear to have any consistent trend over time with respect to the bedrock geology, exhibiting both significant increases and decreases between 1994 to 2023 (see Appendix for Figure 1A).

### ***3.2 Spatial and Temporal Relationship Between pH and DOC***

To evaluate the spatial and temporal patterns associated with pH and DOC, both the high-frequency and synoptic datasets were utilized. The high-frequency dataset was indicative of temporal trends between DOC (calculated from the fDOM) and pH as the same location was continuously monitored while the synoptic dataset was indicative of the spatial relationship between DOC and pH as several sites were monitored on a single day. The temporal relationship between the pH and DOC did not appear to follow a linear trend and most closely resembled a negative relationship (Figure 13).

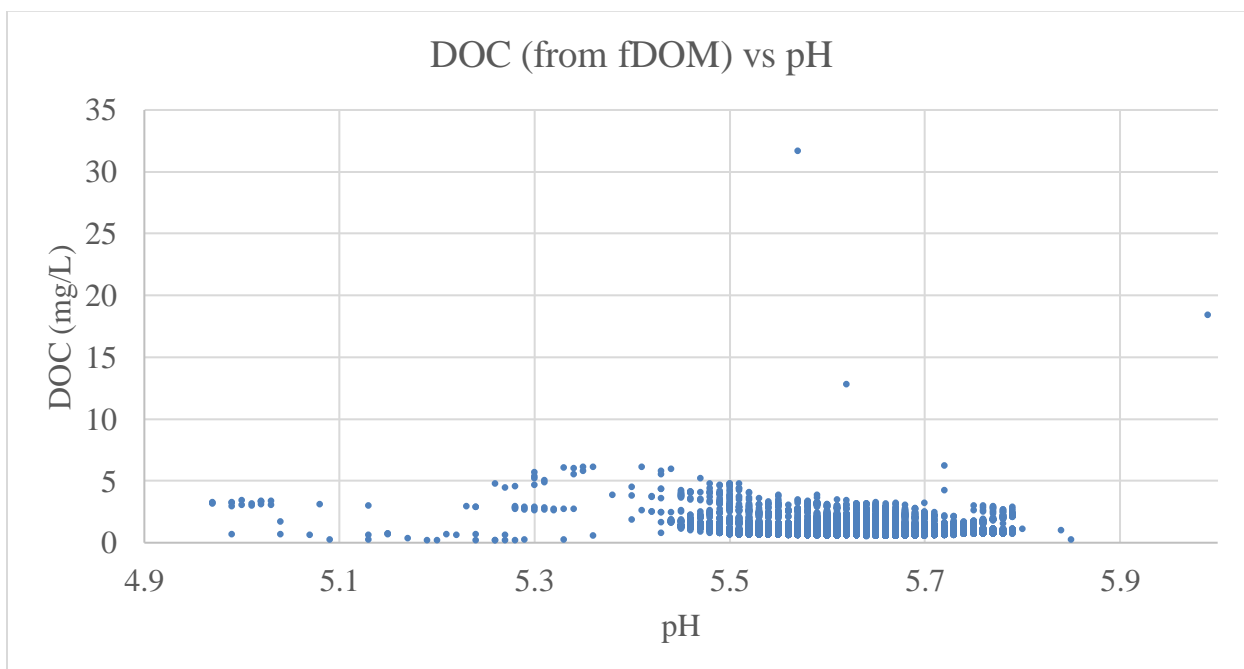


**Figure 13:** DOC (calculated from fDOM) plotted against the pH values from the high-frequency deployment.

The range of the high-frequency DOC values was 0.169 to 31.664 mg/L while the range of pH values was 4.97 to 6.25. There were both high outliers (DOC>1.279 mg/L; pH>5.86) and low outliers (DOC<0.357 mg/L; pH<5.42) with mean values of 0.9025 mg/L and 5.63 for DOC and pH, respectively. Since this dataset contained over 31,000 data points, autocorrelation was avoided by performing statistical analysis on several subsets of 19 randomly selected data points as this is comparable to the number of samples obtained from the synoptic sampling. These results reflected that the slope of DOC vs pH was not significantly different from zero ( $p=0.874$ ) and thus the temporal relationship was not significant. To gain a better understanding of the temporal relationship between pH and fDOM and other factors that can exert influences, the fDOM, pH, and water level were graphed for two storm events in the dataset. During the storm events, as the water level increased, the fDOM increased, peaking on the rising limb while the pH decreased (Figure 14).

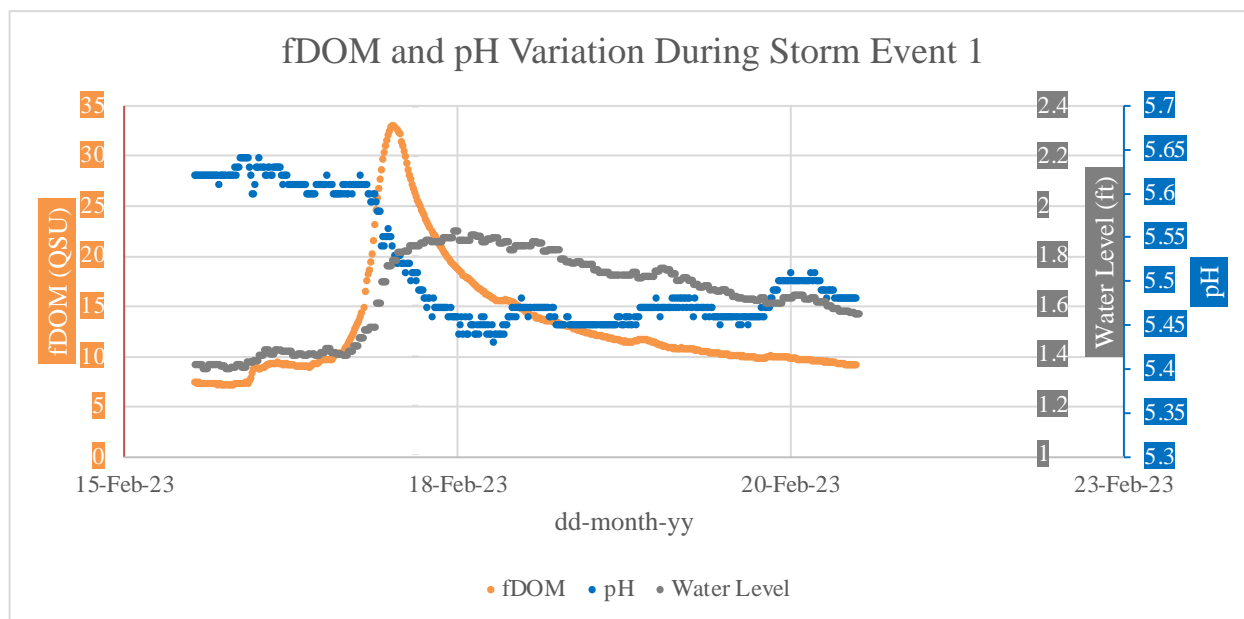


**Figure 14A:** fDOM (QSU), pH, and water level (feet) plotted against time for a storm event occurring from February 16, 2023 to February 20, 2023.

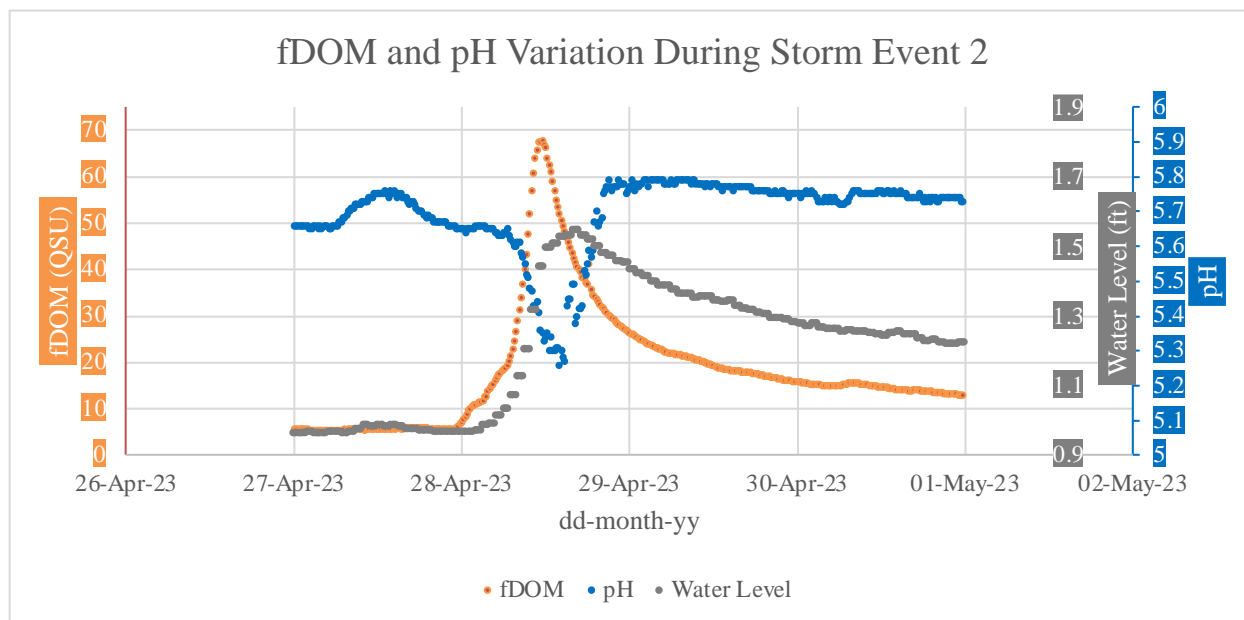


**Figure 14B:** fDOM (QSU), pH, and water level (feet) plotted against time for a storm event occurring from April 27, 2023 to May 1, 2023.

The spatial relationship between DOC and pH also appeared negative but was not statistically significant (slope=-0.1257 mg/L per unit pH;  $R^2=0.0486$ ;  $p=0.379$ ) (Figure 15). From the synoptic dataset, the range of DOC was 0.901 to 1.224 mg/L with a mean value of 1.049 mg/L while the range in pH was 5.12 to 6.07 with a mean value of 5.77 (similar to the temporal range). For the DOC, there were no high outliers (DOC >1.513 mg/L) or low outliers (DOC <0.613 mg/L). For the pH, there were low outliers (pH<5.51) but no high outliers (pH>6.10). In comparison to the temporal data, it appears that the pH ranges were similar. However, the upper range for the temporal DOC was much greater (31.664 mg/L) than that of the spatial DOC (1.224 mg/L).

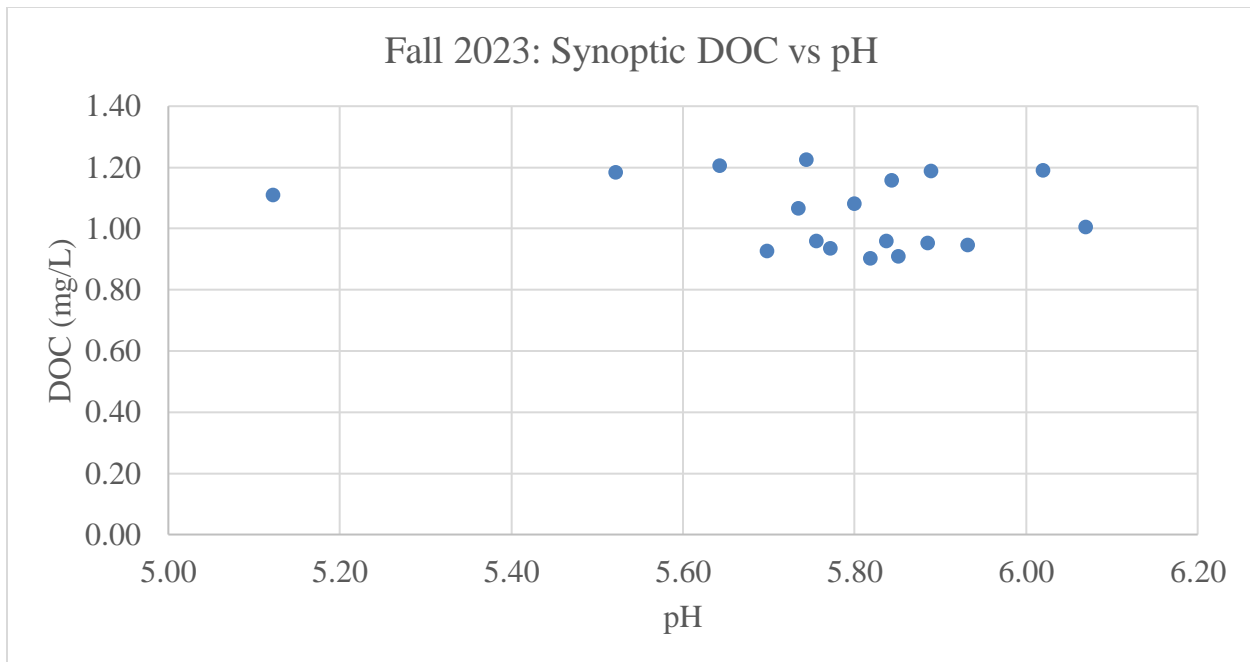


**Figure 15:** The DOC (mg/L) plotted against the pH values from the synoptic sampling with a p-value of 0.379 and  $R^2$  of 0.0486, following the equation  $DOC = -0.1257 \cdot (pH) + 1.7749$ .

## 4. Discussion

### *4.1 Spatial and Temporal Influence of Bedrock Geology on Stream Chemistry*

In studying the influence of bedrock geology on the stream chemistry of Meadow Run over time, it appears that the geology exerted a spatial influence on the initial acidification of the watershed, producing a lasting effect on the stream chemistry. Overall, it was found that there has been minimal impact of the bedrock geology on the stream recovery as demonstrated by similar temporal differences in ANC, pH, and sum of base cations values from the regions containing 0% to 100% Cca. However, greater declines in sulfate were observed with an increasing percentage of Cca, indicating an influence of bedrock on this individual parameter.

The ANC of the site containing 100% Cca improved rather than worsened by a small margin while the sites containing 0% Cca worsened (Figure 6). This suggests that the Antietam Formation potentially had a positive effect on the recovery of ANC. However, if this were the case, a more linear trend between the increase in Cca and the increase in ANC would be expected across all sites. This linearity is not reflected as other sites with varying percentages (20-100%) of Cca showed a similar magnitude of increase to the site at 100%. This indicates that there are covarying factors that may influence the ANC values, contributing to a perceived trend with bedrock geology. Thus, there does not appear to be a pattern between bedrock geology and ANC recovery. In terms of the spatial influence of the bedrock geology on the watershed, the site containing 100% Cca remained chronically acidic, possessing the only negative ANC measured in 1994 and 2023. Additionally, there was a general trend of higher ANC as the percentage of Cca decreased. This suggests that the initial acidification was influenced spatially by the weaker buffer capability of the Antietam Formation as other sites containing a larger amount of the Harpers Formation possessed positive ANC values.

The observation of the minimal impact of bedrock type on stream recovery from 1994 to 2023 was also suggested by the pH values which increased by a similar margin for all sites regardless of bedrock percentage (Figure 7). However, the pH remained the lowest for the site containing 100% Cca by a margin of almost 1 full pH unit when compared to the sites containing 0 to 50% Cca. This indicates that, while the rate of recovery has not been significantly influenced by bedrock type, it does retain a strong long-term control on stream pH.

Although the impact of declines in nitrogen specifically emitted from fossil fuels is harder to quantify as many natural processes result in the release of nitrogen, there were interesting trends observed in the tributaries of the watershed when compared with the main channel. Most sites contained low levels of nitrate and did not experience significant changes from 1994 to 2023 except for those in the 0-40% Cca range (Figure 8). For the sites that did not appear to change significantly, this suggests that the nitrate influences have stayed consistent. For the sites containing 0% Cca that did experience a significant change, covarying factors may have played a role in the observed response. For instance, areas of higher elevation typically possess higher nitrate levels, as observed in the neighboring Paine Run watershed (Scanlon et al., 2010). The sites containing 0% Cca have higher elevations than the site containing 100% Cca, which might be a better explanation for the variation in nitrate concentration. Furthermore, increases in nitrate might be explained by invasive species known to be present in the area (e.g. emerald ash borer) that have impacted plant function, leading to increases in nitrate concentration within the stream (Coughlin, 2016).

The sites with smaller percentages of Cca experienced an increase in sulfate concentration while those with larger percentages experienced decreases from 1994 to 2023 (Figure 9). This indicates that the bedrock geology is likely exerting an influence on the sulfate

concentration. Since sulfate was the main acidifying ion for acid deposition within SHEN, the decreases in emissions after the 1970 Clean Air Act and its amendments in 1990 led to a net release of stored sulfate (Eng and Scanlon, 2021). The retention of sulfate is affected by soil type. It is possible that the sulfate adsorption capacity varies for the sites depending on the bedrock percentage as soil is derived from the bedrock. The sites with larger percentages of Cca likely possess lower adsorption capacities, leading to a greater net release of stored sulfate (Rice et al., 2014). Chloride trends were not expected to vary based on bedrock geology as it is derived from past deposition and associated with decomposition of organic matter rather than soils (Figure 10). The consistently significant decrease in chloride concentration suggests that the chloride stored within the watershed is slowly being depleted as anticipated (Lovett et al., 2005).

All sites experienced a decrease in the sum of base cations except for the site containing 0% Cca (Figure 11). Since the margin of decrease for most sites was comparable, there does not appear to be a pattern with increasing percentage of Cca. Thus, no influence of bedrock geology on the stream recovery from acidification was observed. However, spatially, greater base cation concentrations were associated with lower percentages of Cca in both 1994 and 2023, with the site containing 100% Cca maintaining a persistently lower concentration than all others by about 30  $\mu\text{eq/L}$ . This confirms that the Antietam Formation releases fewer base cations than the Harpers Formation, contributing to the persistent acidity of Meadow Run. For the specific conductivity, it is difficult to quantify the impact of bedrock geology as it depends on the concentration of all ions. However, it does not appear to be directly affected by the bedrock geology as all sites varied to similar degrees regardless of bedrock percentage (Figure 12).

Overall, it appears that the bedrock geology influenced the initial acidification of the watershed as sites containing larger percentages of Cca tended to have lower ANC, pH, and sum

of base cation measurements in 1994 and 2023. However, there does not appear to be a direct influence of the bedrock geology on the recovery from acidification as there were no consistent trends between increasing Cca percentage and changes in ANC, pH, and sum of base cations. Although temporal changes in these variables did not show a pattern with bedrock geology, there was an apparent influence of the bedrock geology on sulfate recovery as sites containing larger amounts of Cca tended to have greater decreases in sulfate from 1994 to 2023. This suggests that the Antietam Formation has a lower adsorption capacity for sulfate than the Harpers Formation, contributing to a greater net release over time.

#### ***4.2 Spatial and Temporal Relationship Between pH and DOC***

For the second research question regarding the exploration of the relationship between pH and DOC, no significant relationship was found spatially or temporally (Figures 13 and 15). It has been previously established in laboratory settings (Yin et al., 1996; Haitzer et al., 2003) and certain field studies (Ekström et al., 2011; Stoken, 2012) that increases in pH lead to increases in DOC; thus, a positive relationship was expected. However, in natural environments, factors other than pH can influence the DOC with the most notable effect being increases in stream discharge due to storm events. This hydrological component often exerts a larger influence on DOC relative to pH. This was observed within the high-frequency dataset during the storm events (Figure 14). For instance, during storm events, the DOC increases with discharge while pH decreases with discharge. This demonstrates that with minor fluctuations in pH, the discharge tends to exert a larger control. Other studies have also demonstrated that forested watersheds with base-poor bedrock geology are susceptible to episodic acidification during storm events (Deyton et al., 2009). Episodic acidification occurs when precipitation causes the mobilization of acid anions from the upper soil horizons and via overland flow,

resulting in brief decreases in pH. In contrast, as the water level increases, a greater magnitude of DOC is mobilized from surficial soils where organic carbon is abundant. Although the pH may have a direct effect on the DOC, the change in the source area mobilized due to storm events likely played a larger role in controlling the DOC measurements for the high-frequency deployment. In a scenario such as the liming where the stream hydrology is constant and the soil pH is altered, this direct positive relationship between DOC and pH is expected to be observed.

While the synoptic sampling data was collected during baseflow conditions, the relationship between DOC and pH was likely influenced by differences in watershed characteristics (e.g. bedrock composition, vegetation, elevation, etc). For instance, in a previous publication documenting differences in pH and DOC in nearby watersheds, a similar inverse relationship was found (lower pH and higher DOC) and was suggested to be a result of differences in soil properties (Riscassi and Scanlon, 2011). For the synoptic dataset, in addition to differences in watershed characteristics, the pH range was less than one full unit (Figure 15). Although pH likely exhibits an effect on DOC, such small variations spatially are not likely to produce a noticeable effect. However, it is possible that a direct relationship still exists and may be observed with larger changes in pH. For example, in previous studies where liming has been performed, the pH varied by 0.5 to 3.5 pH units (Millard et al., 2018). This larger variation in pH is likely to produce a more noticeable effect on the DOC values than smaller natural variations in conditions before liming. As an extension of this study, the DOC and pH monitoring by high-frequency and synoptic data collection will continue after the liming to observe the relationship further with larger changes in pH.

## 5. Conclusion

Despite greater regulations on fossil fuel emissions from the EPA, mountainous streams are still recovering from historic acidification. This study provided a comprehensive analysis of Meadow Run, which is one of the most acidified watersheds in SHEN. By obtaining both high-frequency and synoptic data, the temporal as well as spatial variability of the chemical composition was tracked and analyzed.

The synoptic data from both 1994 and 2023 demonstrated that the bedrock geology had an impact on the initial stream acidification spatially but not on the recovery of the stream from acidification temporally. The spatial influence was observed from the persistent acidity of the sites containing larger percentages of Antietam Formation that possessed lower ANC, pH, and base cation measurements in 1994 and 2023. However, the recovery for most sites in terms of ANC, pH, and base cations was of a similar magnitude with no direct pattern observed, suggesting that the bedrock geology had little if any influence temporally on changes in stream acidity. The bedrock type did exert an influence on temporal trends in sulfate, indicating that soils derived from Antietam Formation, where greater declines were observed, likely possess a lower adsorption capacity. For the relationship between DOC and pH, the high-frequency data from 2022-2023 and synoptic data from 2023 demonstrated that there was no significant observable relationship. This was likely because such small natural variations in pH are unlikely to generate an effect to the same extent as the hydrological influences on DOC temporally and the influences of the watershed characteristics spatially. However, after the liming, there will be a larger change in pH while other influences are held constant, which may provide an observable relationship between DOC and pH. Thus, this site will continue to be monitored with high-frequency and synoptic data to better understand the relationship between DOC and pH.

## References

1. APHA. 1992. *Standard methods for the examination of water and wastewater*. 18<sup>th</sup> ed. American Public Health Association, Washington, DC. River Watch Network. 1992. Total alkalinity and pH field and laboratory procedures (based on University of Massachusetts Acid Rain Monitoring Project).
2. Barron, J. J., & Ashton, C. (2022). The Effect of Temperature on Conductivity Measurement . *Reagecon*. <https://doi.org/10.2514/6.2022-0665>.vid
3. Bulger, A. J., B. J. Cosby, C. A. Dolloff, K. N. Eshleman, J. R. Webb, and J. N. Galloway 1999 SNP:FISH, Shenandoah National Park: Fish in sensitive habitats. Project final report to National Park Service. University of Virginia, Charlottesville, VA. Volumes 1-4.
4. Burns, D. A., J. A. Lynch, B. J. Cosby, M. E. Fenn, J. S. Baron, and US EPA Clean Air Markets Division 2011 National acid precipitation assessment program report to Congress 2011: An Integrated assessment. National Science and Technology Council, Washington, DC.
5. Coughlin, K. M. (2016). An Investigation and Quantification of Nitrogen Sources and Sinks in Shenandoah National Park, Virginia [Unpublished M.S. Thesis]. University of Virginia.
6. DOI (U.S. Department of the Interior). (2021). *Environmental Assessment - Shenandoah National Park Meadow Run Watershed Restoration*. National Parks Service. <https://parkplanning.nps.gov/document.cfm?parkID=274&projectID=74048&documentID=109570>

7. Ekström, S. M., E. S. Kritzberg, D. B. Kleja, N. Larsson, P. A. Nilsson, W. Graneli, and B. Bergkvist (2011), Effect of acid-deposition on quantity and quality of dissolved organic matter in soil-water, *Environ. Sci. Technol.*, 45(11), 4733-4739, doi:10.1021/es104126f.
8. Eng, L. E., & Scanlon, T. M. (2021). Comparison of Northeastern and Southeastern U.S. watershed response to the declines in atmospheric sulfur deposition. *Atmospheric Environment*, 253, 118365. <https://doi.org/10.1016/j.atmosenv.2021.118365>
9. Graveland, J. 1998 “Effects of acid rain on bird populations.” *Environmental Reviews* 6:41–54.
10. Haitzer, M., G. R. Aiken, and J. N. Ryan (2003), Binding of mercury(II) to aquatic humic substances: influence of pH and source of humic substances, *Environ. Sci. Technol.*, 37, 2436-2441, doi:10.1021/es026291o.
11. Harmon, P. A., Riscassi, A. L., Scanlon, T. M., Galloway, J. N., Demarest, D., & May, C. L. (2021). The impacts of stream acidification on fish assemblages: Assessing three decades of recovery in Shenandoah national park. *Global Ecology and Conservation*, 26. <https://doi.org/10.1016/j.gecco.2020.e01386>
12. Hoffmeister, S., Murphy, K. R., Cascone, C., Ledesma, J. L., & Köhler, S. J. (2020). Evaluating the accuracy of two *in situ* optical sensors to estimate DOC concentrations for drinking water production. *Environmental Science: Water Research & Technology*, 6(10), 2891–2901. <https://doi.org/10.1039/d0ew00150c>
13. Jastram, J. D., C. D. Snyder, N. P. Hitt, and K. C. Rice 2013 “Synthesis and interpretation of surface water quality and aquatic biota data collected in Shenandoah National Park, Virginia, 1979-2009.” US Geological Survey Scientific Investigations Report 2013-5157, Reston, VA.

14. Kaufmann, P. R., Herlihy, A. T., Mitch, M. E., Messer, J. J., & Overton, W. S. (1991). Stream Chemistry in the Eastern United States: 1. synoptic survey design, acid-base status, and regional patterns. *Water Resources Research*, 27(4), 611–627.  
<https://doi.org/10.1029/90wr02767>
15. Lawrence, G. B., Burns, D. A., & Riva-Murray, K. (2016). A new look at liming as an approach to accelerate recovery from acidic deposition effects. *Science of The Total Environment*, 562, 35–46. <https://doi.org/10.1016/j.scitotenv.2016.03.176>
16. Millard, G. D., Driscoll, C. T., Burns, D. A., Montesdeoca, M. R., & Riva-Murray, K. (2018). Response of Mercury in an Adirondack (NY, USA) forest stream to Watershed Lime Application. *Environmental Science: Processes & Impacts*, 20(4), 607–620.  
<https://doi.org/10.1039/c7em00520b>
17. Rice, K. C., Scanlon, T. M., Lynch, J. A., & Cosby, B. J. (2014). Decreased atmospheric sulfur deposition across the southeastern U.S.: When will watersheds release stored sulfate? *Environmental Science & Technology*, 48(17), 10071–10078.  
<https://doi.org/10.1021/es501579s>
18. Riscassi, A. L., & Scanlon, T. M. (2011). Controls on stream water dissolved mercury in three mid-appalachian forested headwater catchments. *Water Resources Research*, 47(12). <https://doi.org/10.1029/2011wr010977>
19. Riscassi, A. L., Scanlon, T., Maben, S., & Galloway, J. (2020). *Shenandoah Watershed Study-Virginia Trout Stream Sensitivity Study (Swas-VTSSS): Stream Water Quality and Hydrologic Monitoring Data for Mid-Appalachian Headwater Streams*.  
<https://doi.org/10.22541/au.160010828.85236114>

20. Scanlon, T. M., Ingram, S. M., & Riscassi, A. L. (2010). Terrestrial and in-stream influences on the spatial variability of nitrate in a forested headwater catchment. *Journal of Geophysical Research: Biogeosciences*, 115(G2).  
<https://doi.org/10.1029/2009jg001091>
21. Shao, S., Driscoll, C. T., Sullivan, T. J., Burns, D. A., Baldigo, Barry P., Lawrence, G. B., & McDonnell, T. C. (2020). The response of stream ecosystems in the Adirondack Region of New York to historical and future changes in atmospheric deposition of sulfur and nitrogen. *Science of The Total Environment*, 716, 137113.  
<https://doi.org/10.1016/j.scitotenv.2020.137113>
22. Sharpe, P. J. and J. Cummings. (2019). Sampling plan for supplemental surficial soil assessment of the Meadow Run watershed in Shenandoah National Park, VA (unpublished data set)
23. Stoken, O.M. (2012). Regional and local controls on dissolved mercury and dissolved organic carbon in streams [Unpublished M.S. Thesis]. University of Virginia.
24. United States Environmental Protection Agency (EPA) (2010). Title IV, section 408.  
<https://www.epa.gov/acidrain/acid-rain-program>
25. U.S. Energy Information Administration - EIA - independent statistics and analysis. Electricity in the U.S. - U.S. Energy Information Administration (EIA). (2022).  
<https://www.eia.gov/energyexplained/electricity/electricity-in-the-us.php#:~:text=Fossil%20fuels%20are%20the%20largest,gas%20turbines%20to%20generate%20electricity>.

26. VADEQ (Virginia Department of Environmental Quality). (2020) 305(b)/303(d) Water Quality Assessment Integrated Report. <https://www.deq.virginia.gov/our-programs/water/water-quality/assessments/integrated-report>
27. Wagner, R. J., Boulger, R. W., Oblinger, C. J., & Smith, B. A. (2006). Guidelines and standard procedures for continuous water-quality monitors: Station operation, record computation, and Data Reporting. *Techniques and Methods*.  
<https://doi.org/10.3133/tm1d3>
28. Yin, Y. J., H. E. Allen, Y. M. Li, C. P. Huang, and P. F. Sanders (1996), Adsorption of mercury(II) by soil: Effects of pH, chloride, and organic matter, *J. Environ. Qual.*, 25(4), 837-844, doi:10.2134/jeq1996.00472425002500040027x.
29. YSI. (2020). Exo User Manual.  
<https://www.ysi.com/file%20library/documents/manuals/exo-user-manual-web.pdf>

## Appendix

### Table 1A EXO2 Sonde Calibration Parameters (adapted from YSI, 2020)

Sensor	Point(s) for Calibration
ODO	1. Water-saturated air (calibration cup filled with 1/8 inch of DI water and sensors saturated 10-15 minutes)
fDOM	1. DI water 2. 300 microg/L standard (made fresh before each calibration)
pH	1. pH of 4 standard 2. pH of 7 standard
Turbidity	1. DI water 2. YSI 124 FNU Standard
Conductivity/Temperature	1. 1000 $\mu$ S/cm standard

### Table 2A SWAS Laboratory Procedures

Measurement	Method	Equipment	Citation
ANC	11-point automated Gran titration	Metrohm 809 titration system; 100 ml open-system samples and 0.01 N HCl titrant	U.S. EPA, 1987. Handbook of Methods for Acid Deposition Studies: Laboratory Analyses for Surface Water Chemistry. EPA 600/4-87/026. Section 5.; Gran, G., 1952. Determination of the Equivalence Point in Potentiometric Titrations, Part II. Analyst, v. 77, pp. 661-671.
pH	automated potentiometric measurement	Metrohm 809 titration system; open-system samples in laboratory	U.S. EPA, 1987. Handbook of Methods for Acid Deposition Studies: Laboratory Analyses for Surface Water Chemistry. EPA 600/4-87/026. Section 5.; Gran, G., 1952. Determination of the Equivalence Point in Potentiometric Titrations, Part II. Analyst, v.77, pp. 661-671.
Base Cations	ion chromatography	Dionex Model ICS 3000 Ion Chromatograph	ASTM Method D 6919-03: Determination of Dissolved Alkali and Alkaline Earth Cations and Ammonium in Water and Wastewater by Ion Chromatography: ASTM International. 2003. Annual Book of ASTM Standards, Section 11, Water and Environmental Technology, Volume 11.02. ASTM International.
Acid Anions	ion chromatography	Dionex Model ICS 3000 Ion Chromatograph	U.S. EPA Office of Ground Water and Drinking Water/Technical Support Center; 1997; Methods for the Determination of Organic and Inorganic Compounds in Drinking Water, Volume 1 (EPA/815-R-00-014); EPA Method 300.1: Determination of Inorganic Anions in Drinking Water by Ion Chromatography; U.S. EPA; EPA/815-R-00-014.
Silica	flow injection analysis	Lachat QuikChem 8500 Series 2	Roy McKnight; 13 Sep 2000 (rev.); Determination of Silica in Waters by Flow Injection Analysis: QuikChem Method 10-114-27-1-A; Lachat Instruments; 10-114-27-1-A
Dissolved Organic Carbon	UV/persulfate oxidation and infrared detection	Teledyne-Tekmar FUSION TOC Analyzer	EPA/600/R-05/055; 2003; EPA Method 415.3, Revision 1.0: Determination of Total Organic Carbon and Specific UV Absorbance at 254 nm in Source Water and Drinking Water

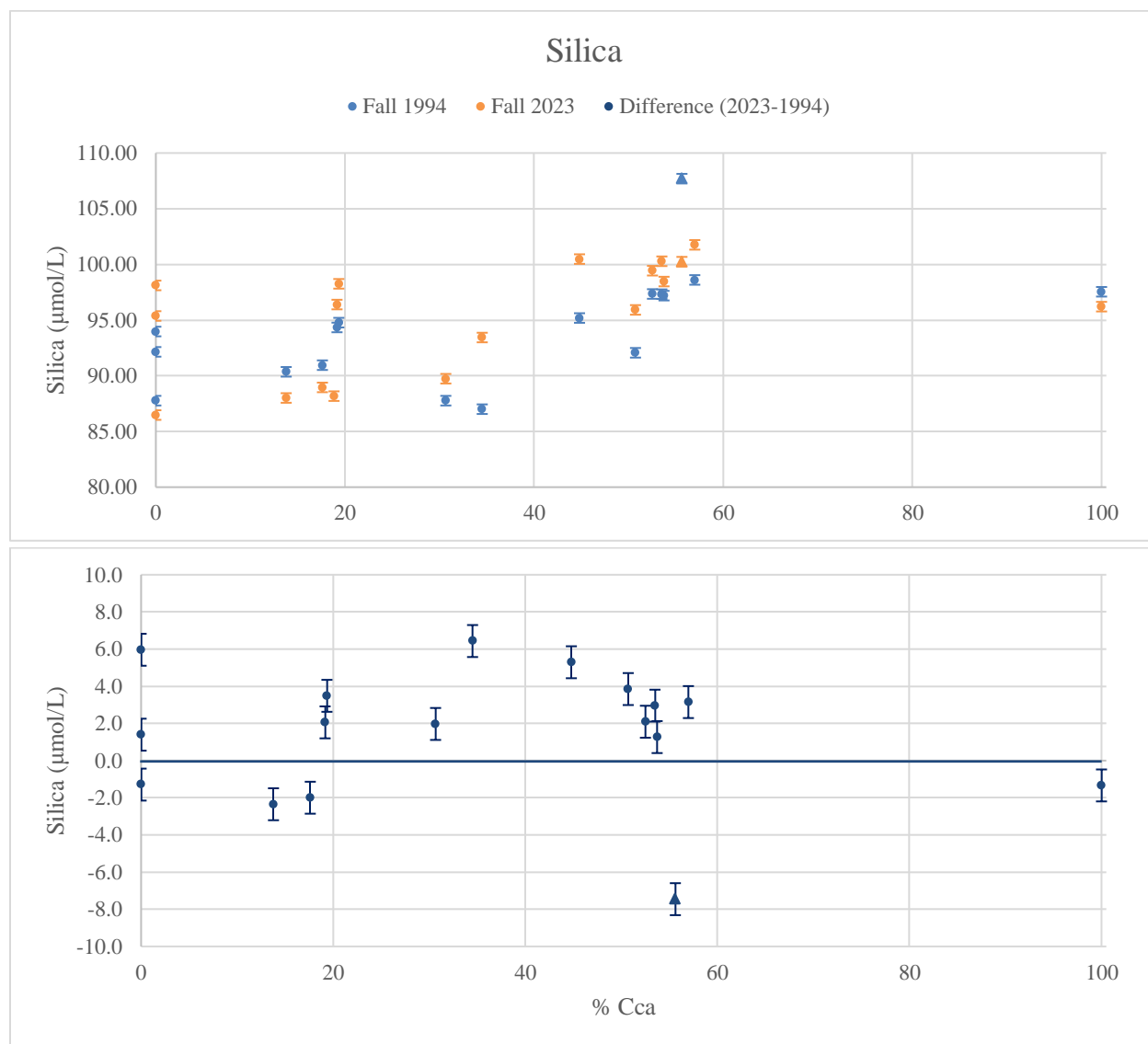


**Figure 1A:** Silica ( $\mu\text{mol/L}$ ) from fall 1994 (blue) and fall 2023 (orange) plotted along with the difference between 2023 and 1994 (dark blue) against the percentage of Cca. The error bars of  $\pm 0.43$  ( $>17 \mu\text{eq/L}$ ) for fall 1994 and 2023 were obtained from the average values for 2022. The error bars for the difference were the sum of the fall 1994 and 2023 error values. The triangles represent site VT36 where the high-frequency data has been collected.